31st International Conference Nuclear Energy for New Europe
NENE 2022 September 12-15 PORTOROŽ SLOVENIA

STRAIN LOCALIZATION IN AUSTENITIC STAINLESS STEEL DUE TO HYDROGEN CONCENTRATION

Amirhossein Lame Jouybari [a,b]
[a] Faculty of Mathematics and Physics, University of Ljubljana
Jadranska ulica 19
SI-1000, Ljubljana, Slovenia
amirhossein.lame@student.fmf.uni-lj.si, amirhossein.lame@ijs.si

Samir El Shawish [a,b], **Leon Cizelj** [a,b]
[b] Jožef Stefan Institute
Jamova cesta 39
SI-1000, Ljubljana, Slovenia
samir.elshawish@ijs.si, leon.cizelj@ijs.si

ABSTRACT

The aging of austenitic stainless steel in the harsh environment of the Light Water Reactor is highly sensitive to Stress Corrosion Cracking. The presence of hydrogen in such steels can change their microstructure and affect the mobility of dislocations, which may result in the deterioration of mechanical properties like embrittlement and strain localization.

This preliminary study is concerned with the formation of strain localization in the crystal plasticity finite element model of the austenitic stainless steel polycrystal due to hydrogen concentration. In this framework, polycrystals are generated by Voronoi tessellation topologies with zero crystallographic texture. Hydrogen effect is considered in the decomposition of the deformation gradient into elastic, hydrogen, and plastic parts. A rate-independent form of constitutive equations is derived and implemented numerically in the User MATerial subroutine in Abaqus software. Finally, the effect of hydrogen concentrations is studied in a polycrystalline aggregate in a series of uniaxial tension simulations.

1 INTRODUCTION

Austenitic stainless steel (SS) alloys are commonly used in internal structures of nuclear reactors (internals) because of their high resistance to corrosion, irradiation, and excellent mechanical properties. These alloys need to perform in harsh environment, for example at temperatures of 300 - 370℃, typical for lower internals in Light Water Reactors (LWR), at neutron fluxes of 10^{14} – 10^{15} neutron/cm^2/s, and at coolant flow rates of $\simeq 10^4$ kg s^{-1} [1]. Physically, the aging of internals appears as cracking, which is driven by the stress corrosion cracking (SCC) mechanism. The hydrogen atoms from primary coolant circuit of LWR increase the SCC sensitivity [1].

Austenitic SS exhibits periodic arrangement of atoms in space and forms Face Centred Cubic (FCC) crystal lattice [1]. Various aspects of FCC crystal phenomena, such as strain and stress localization, texture evolution, work hardening and void formation, have been analysed in the literature by the emergence of crystal plasticity theory using the concept of a dislocation as a linear lattice defect or discontinuity [2, 3, 4].

A finite element method is a strong numerical tool which has been widely established for studying the mechanical behaviour of crystalline materials. Voronoi polycrystalline aggregates have been assigned to estimate inter-granular normal stress distributions as an important ingredient towards Inter-Granular Stress Corrosion Cracking (IGSCC) [5, 6, 7].

Experimental observations [8] on hydrogen-charged polycrystalline nickel show an increase of dislocation's mobility (higher velocities) and accordingly a decrease of stress. Furthermore, the amount of deformation in a localized region adjacent to the fractured surface is eventually increased which is called Hydrogen Enhanced Localized Plasticity (HELP) [8]. However, the initial activation of immobile dislocations tends to increase with hydrogen concentration, which is related to the loss of ductility and increase of embrittlement. For example, the yield strength is notably increased in hydrogen-charged specimens under uniaxial tension (increase of 25% for nickel and 30% for austenitic SS [8, 9, 10, 11]) and the hardening's stages react in different manner for hydrogen-free and for hydrogen-charged FCC crystal specimens under uniaxial tension.

This study attempts to derive crystal plasticity rate-independent (objective) constitutive equations and proposes a rate-independent tangent modulus between the objective tensors in the constitutive equations for numerical implementation. In addition, the study tries to incorporate hydrogen concentration parameters in the rate-independent constitutive equations by the consistency condition and thermodynamics of hydrogen atoms. Finally, all the derivations are implemented into finite element code Abaqus through the User MATerial subroutine to simulate stress-strain behaviour of hydrogen-charged austenitic SS specimen under tensile loading and finite hydrogen concentration.

2 CRYSTAL PLASTICITY CONSTITUTIVE EQUATIONS

Austenitic stainless steel crystallizes into a FCC structure. Crystal dislocations glide along the 12 slip systems, $\{111\}\langle 110\rangle$, and a trail of them is visible in each term of the constitutive equations [12]. In general, the constitutive equations of isothermal large-strain elastoplasticity are expressed in the rate form, $\overset{*}{\underset{\sim}{\sigma}} = F(\underset{\sim}{D}, \Xi)$, where $\overset{*}{\underset{\sim}{\sigma}}$ represents an objective stress rate, $\underset{\sim}{D}$ is the symmetric part of the velocity gradient and Ξ denotes the internal variables [12].

Tangent modulus $\underset{\approx}{L}$ (also tangent stiffness matrix) is required in finite element simulations at each time increment to describe the local material behaviour. It assigns a stress increment to a strain increment and is of fundamental importance for the numerical determination of the equilibrium state. For increasingly sophisticated material models the tangent modulus can be approximated only numerically. In the following, a derivation of the tangent modulus is presented in a finite strain framework[1].

2.1 Elastic rate-independent tangent modulus

The elastic behaviour of the material is distinguished from its plastic counterpart by a concave yield surface concerning the Cauchy stress tensor. This scalar-valued tensor function indicates the elastic regime whenever the stress state is located inside the yield surface. The linear-elastic constitutive equation for the FCC crystal with cubic symmetry is written as [12],

$$\underset{\sim}{\sigma} = \underset{\approx}{C} : \underset{\sim}{\varepsilon} \tag{1}$$

[1] Symbol notation is introduced in Tab. 2 in Appendix.

where the non-zero coefficients of elasticity tensor in Voigt notation are $c_{11} = c_{22} = c_{33}, c_{44} = c_{55} = c_{66}$, $c_{12} = c_{13} = c_{23}$. By applying the time derivative to the linear elastic constitutive equation, the Cotter-Rivilin objective rate-independent form of the tangent modulus in the current configuration is derived as [12],

$$\overset{*}{\underset{\sim}{\tau}} = \underset{\approx}{L}^{e\tau} : \underset{\sim}{D}^{e} \tag{2}$$

where $\overset{*}{\underset{\sim}{\tau}} = \dot{\underset{\sim}{\tau}} + \underset{\sim}{\tau} . (\underset{\sim}{W} - \underset{\sim}{W}^{p}) - (\underset{\sim}{W} - \underset{\sim}{W}^{p}) . \underset{\sim}{\tau}$ is the Cotter-Rivilin objective rate, ${L^{e\tau}}_{ijkl} = c_{ijkl} + \frac{1}{2}(\tau_{il}\delta_{jk} + \tau_{ik}\delta_{jl} + \tau_{jl}\delta_{ik} + \tau_{jk}\delta_{il})$ is the tangent modulus, $\underset{\sim}{\tau}$ is the Kirchhoff stress tensor, $D^{e}_{ij} = \frac{1}{2}(\frac{\partial v_i}{\partial x_j} - \frac{\partial v_j}{\partial x_i})$. By applying some algebraic manipulations, the final form in terms of the Zaremba-Jaumann objective stress rate is obtained [12],

$$\overset{\nabla}{\underset{\sim}{\tau}} = \underset{\approx}{L}^{e\tau} : \underset{\sim}{D}^{e} + \underset{\sim}{\tau} . \underset{\sim}{W}^{p} - \underset{\sim}{W}^{p} . \underset{\sim}{\tau} \tag{3}$$

where[2] $\underset{\sim}{W} = \mathrm{skew}(\nabla_{\underset{\sim}{x}} \underset{\sim}{v}(\underset{\sim}{x}, t))$, and $\underset{\sim}{W}^{p} = \sum_{\alpha=1}^{12} \dot{\gamma}^{\alpha}(t) \mathrm{skew}(\underset{\sim}{s}_0^{\alpha} \otimes \underset{\sim}{m}_0^{\alpha})$.

2.2 Plastic rate-independent tangent modulus

Theory of finite inelastic (plastic, viscose, etc.) strain is based on the fundamental assumption where the total deformation gradient is decomposed into a product of purely plastic (intermediate configuration) and elastic (final configuration) terms [12]. A unique intermediate configuration must be isoclinic (orientation-preserving) which means no change of lattice orientation takes place during plastic deformation. However, the orientations may eventually change in the current configuration by elastic deformation.

Physically, plastic deformation occurs by gliding of dislocations in active slip systems α, which can be described by plastic velocity gradient[3] [12]

$$\underset{\sim}{L}_{i}^{p} = \sum_{\alpha=1}^{12} \dot{\gamma}^{\alpha}(t) \underset{\sim}{s}_0^{\alpha} \otimes \underset{\sim}{m}_0^{\alpha}. \tag{4}$$

The Jaumann objective stress rate is expressed in terms of shear strain rate ($\dot{\gamma}$) and symmetric part of the velocity gradient ($\underset{\sim}{D}$),

$$\begin{aligned} \overset{\nabla}{\underset{\sim}{\tau}} = \underset{\approx}{L}^{e\tau} : \underset{\sim}{D} - \sum_{\alpha=1}^{12} \dot{\gamma} \, [\underset{\approx}{L}^{e\tau} : \mathrm{sym}(\underset{\sim}{s}^{\alpha} \otimes \underset{\sim}{m}^{\alpha}) + \mathrm{skew}(\underset{\sim}{s}^{\alpha} \otimes \underset{\sim}{m}^{\alpha}) . \underset{\sim}{\tau} \\ - \underset{\sim}{\tau} . \mathrm{skew}(\underset{\sim}{s}^{\alpha} \otimes \underset{\sim}{m}^{\alpha})]. \end{aligned} \tag{5}$$

The rate of Kirchhoff stress tensor, $\dot{\tau}^{\alpha}$, within each slip system is given by considering two constrains, the yield condition ($\dot{\phi} = \dot{\tau}^{\alpha} - {\dot{\tau}^{\alpha}}_{cr} \leq 0$) with respect to critical resolved stress as a strength in the associated slip system, ${\dot{\tau}^{\alpha}}_{cr}$, and $\dot{\phi}$ as a rate of yield surface, and the consistency condition (if $\dot{\phi} = 0$ then $\dot{\gamma}^{\alpha} \geq 0$),

$$\begin{aligned} \dot{\tau}^{\alpha} = \Big(\underset{\approx}{L}^{e\tau} : s \, \mathrm{ym}(\underset{\sim}{s}^{\alpha} \otimes \underset{\sim}{m}^{\alpha}) + \mathrm{skew}(\underset{\sim}{s}^{\alpha} \otimes \underset{\sim}{m}^{\alpha}) . \underset{\sim}{\tau} - \underset{\sim}{\tau} . \mathrm{skew}(\underset{\sim}{s}^{\alpha} \otimes \underset{\sim}{m}^{\alpha}) \Big) \\ : \Big(\underset{\sim}{D} - \sum_{\beta=1}^{12} \dot{\gamma}^{\beta} \mathrm{sym}(\underset{\sim}{s}^{\beta} \otimes \underset{\sim}{m}^{\beta}) \Big). \end{aligned} \tag{6}$$

[2] ∇ is the gradient operator in the current configuration.

[3] Where $\underset{\sim}{s}_0^{\alpha}$ is the slip direction and $\underset{\sim}{m}_0^{\alpha}$ is the normal to the slip plane in slip system α in the reference configuration, and $\underset{\sim}{s}^{\alpha} = \underset{\sim}{F}^{e} . \underset{\sim}{s}_0^{\alpha}$ and $\underset{\sim}{m}^{\alpha} = \underset{\sim}{m}_0^{\alpha} . \underset{\sim}{F}^{e-1}$ in the current configuration.

By considering the consistency condition, the matrix form of the relation between the shear strain rate and symmetric part of velocity gradient is derived[4],

$$\dot{\gamma}^{\alpha} = \sum_{\beta=1}^{12}\Big(\sum_{\alpha=1}^{12}\big(\underset{\approx}{L}^{e\tau} : s\,\mathrm{ym}(\underline{s}^{\alpha}\otimes\underline{m}^{\alpha}) + \mathrm{skew}(\underline{s}^{\alpha}\otimes\underline{m}^{\alpha}).\underline{\underline{\tau}} - \underline{\underline{\tau}}.\,\mathrm{skew}(\underline{s}^{\alpha}\otimes\underline{m}^{\alpha})\big) : s\,\mathrm{ym}(\underline{s}^{\beta}\otimes\underline{m}^{\beta}) + h^{\alpha\beta}\Big)^{-1} : \big(\underset{\approx}{L}^{e\tau} : s\,\mathrm{ym}(\underline{s}^{\alpha}\otimes\underline{m}^{\alpha}) + \mathrm{skew}(\underline{s}^{\alpha}\otimes\underline{m}^{\alpha}).\underline{\underline{\tau}} - \underline{\underline{\tau}}.\,\mathrm{skew}(\underline{s}^{\alpha}\otimes\underline{m}^{\alpha})\big) : \underline{\underline{D}} \tag{7}$$

or, using shorter notation,

$$\dot{\gamma}^{\alpha} = \Big(\sum_{\beta=1}^{12}\Psi^{\alpha\beta}\,\Omega^{\beta}\Big) : \underline{\underline{D}}. \tag{8}$$

The rate-independent plastic tangent modulus is derived,

$$\underset{\approx}{L}^{J} = \underset{\approx}{L}^{e\tau} - \Big(\sum_{\alpha=1}^{12}\sum_{\beta=1}^{12}\Psi^{\alpha\beta}\,.\Omega^{\alpha}.\Omega^{\beta}\Big). \tag{9}$$

Finally, the rate-independent constitutive equation is given by the rate-independent tangent modulus,

$$\overset{\nabla}{\underline{\underline{\tau}}} = \underset{\approx}{L}^{J} : \underline{\underline{D}}. \tag{10}$$

The elastic ($\underset{\approx}{L}^{e\tau}$) and plastic ($\underset{\approx}{L}^{J}$) rate-independent tangent moduli have been implemented in the Abaqus UMAT subroutine using the hardening law from the following section.

2.3 Hardening model

Plastic deformation produces dislocations which can glide along the 12 slip systems of the FCC crystal. The first slip can be predicted by the optimally oriented slip system by finding the corresponding maximum Schmid factor. With time (or deformation), crystal orientations may change due to elastic deformation, which may activate and/or produce dislocations in other slip systems. Therefore, interactions between dislocations must be considered during plastic simulation. This phenomenon is called "dislocation hardening" and there exists different types of models associated with it. This study considers the Bassani & Wu hardening model that includes both the active self[5] and latent[6] hardenings and affects the critical resolved shear stress by the consistency condition [13],

$$\dot{\tau}_{cr}^{\alpha} = \sum_{\beta=1}^{12} h^{\alpha\beta}\dot{\gamma}^{\beta} \tag{11.a}$$

$$h^{\alpha\alpha} = \Big[(h_0 - h_s)\,sech^2\Big(\frac{h_0 - h_s}{\tau_I - \tau_0}\gamma^{\alpha}\Big) + h_s\Big]\Big[1 + \sum_{\substack{\beta=1\\ \beta\neq\alpha}}^{12} f_{\alpha\beta}\,tanh\Big(\frac{\gamma^{\beta}}{\gamma_0}\Big)\Big] \tag{11.b}$$

$$h^{\beta\alpha} = q h^{\alpha\alpha} \qquad \alpha \neq \beta \tag{11.c}$$

where $q \in [0,0.3]$ and $f_{\alpha\beta}$ is a parameter associated with various dislocation interactions, τ_0 is the initial critical resolved shear stress at the onset of plastic deformation, τ_I is the Stage I stress due to large plastic flow initiation, h_0 is the hardening modulus associated with τ_0, h_s is the easy dislocation glide hardening, γ_0 denotes the amount of slip when the interaction of

[4] $h^{\alpha\beta}$ is a component of the hardening model which is discussed in the next section.
[5] Interaction between dislocations within the same slip system.
[6] Interaction between dislocations from different slip systems.

dislocations from different slip systems reaches peak strength, $sech$ is the secant hyperbolic, and γ^{α} is the shear strain in the α slip system.

2.4 Hydrogen concentration

Hydrogen solute atoms interact with dislocations and reside in the microstructure of the austenitic SS. The multiplicative decomposition of the deformation gradient is proposed in terms of the elastic $\underset{\sim}{F}^{e}$, plastic $\underset{\sim}{F}^{p}$, and hydrogen-associated[7] part $\underset{\sim}{F}^{h}$ [14],

$$\underset{\sim}{F} = \underset{\sim}{F}^{e}.\underset{\sim}{F}^{h}.\underset{\sim}{F}^{p}. \tag{12}$$

Hydrogen atoms reside at two locations in the crystal lattices: (i) normal interstitial lattice sites (NILS) and (ii) trapping sites associated with dislocation movements. The quantities in each hydrogen location are always in equilibrium, based on the theory of Oriani [15],

$$\frac{\theta_T^{\alpha}}{1-\theta_T^{\alpha}} = \frac{\theta_L}{1-\theta_L} K_T \tag{13}$$

where θ_L denotes the occupancy of lattice sites, θ_T^{α} is the respective occupancy of the trap sites in the slip system α, and K_T is the equilibrium constant. Accordingly, the normal NILS concentration and normal trap concentration (atoms per volume) [14],

$$\begin{cases} c_L = C_L/N_L \\ c_T^{\alpha} = C_T^{\alpha}/N_L \end{cases}. \tag{14}$$

where N_L is the number of lattice atoms per unit of lattice volume calculated by Avogadro's number and the molar volume of the lattice. It is assumed that each slip system has only one trap site associated with the gliding dislocations [18]. This assumption provides the relation between the dislocation density on the slip system α and the number of trap sites [14],

$$\rho^{\alpha} = N_T^{\alpha} b. \tag{15}$$

Furthermore, the dislocation density is expressed in terms of the Burgers vector (b) and critical resolved shear stress [14],

$$N_T^{\alpha} = \left(\frac{\tau_{cr}^{\alpha}}{\tilde{\alpha} G}\right)^2 \frac{1}{b^3}. \tag{16}$$

Although hydrogen atoms can diffuse in polycrystalline materials, recent simulation results of hydrogen diffusion in nickel polycrystals indicate less than 10% spatial variation of total hydrogen concentration [16]. Therefore, hydrogen diffusion is neglected in this study. This makes the total hydrogen concentration fixed at all times and at each material point of the body, resulting in the following hydrogen equilibrium equation [14],

$$c_L + \sum_{\alpha} c_T^{\alpha} = c_0. \tag{17}$$

Finally, the effect of hydrogen concentration is employed in the critical shear stress rate, Eq. (11.a), by the following modification of the hardening law [14],

$$h_H^{\alpha\beta} = (1 + H_c c_T^{\alpha}) h^{\alpha\beta}. \tag{18}$$

[7] In general, the hydrogen deformation contains both dilatational (volumetric) strain ($\mathrm{tr}(\underset{\sim}{\varepsilon}^{h}) \neq 0$) and deviatoric (shear) part ($\mathrm{dev}(\underset{\sim}{\varepsilon}^{h}) = \underset{\sim}{\varepsilon} - 1/3\mathrm{tr}(\underset{\sim}{\varepsilon}^{h}) \simeq 0$). But it is experimentally observed that the hydrogen-deformation gradient is purely dilatational.

Similarly, the effect of hydrogen on the initial critical shear stress (τ_0) is modelled linearly as $(\tau_0^\alpha)_H = (1 + T_C c_0^\alpha)\tau_0$, where c_0^α is the trap hydrogen concentration at initial time step.

To conclude, the effect of hydrogen is described by 1+12 additional variables (c_L and c_T^α), which are controlled by three newly introduced (hydrogen) parameters ($H_c < 0$, $T_c > 0$, c_0).

3 VALIDATION

In this section, the implementation of the derived constitutive equations in Abaqus UMAT subroutine is validated by performing a tensile test of Ni single crystal bar model along the [135] crystal direction. In Fig. 1 a comparison is shown between the simulation results of this and a previous study [17]. Same elasto-plastic material and hydrogen parameters are used in the comparison (see [17] for details). A good agreement is observed, which validates the implementation of the UMAT code.

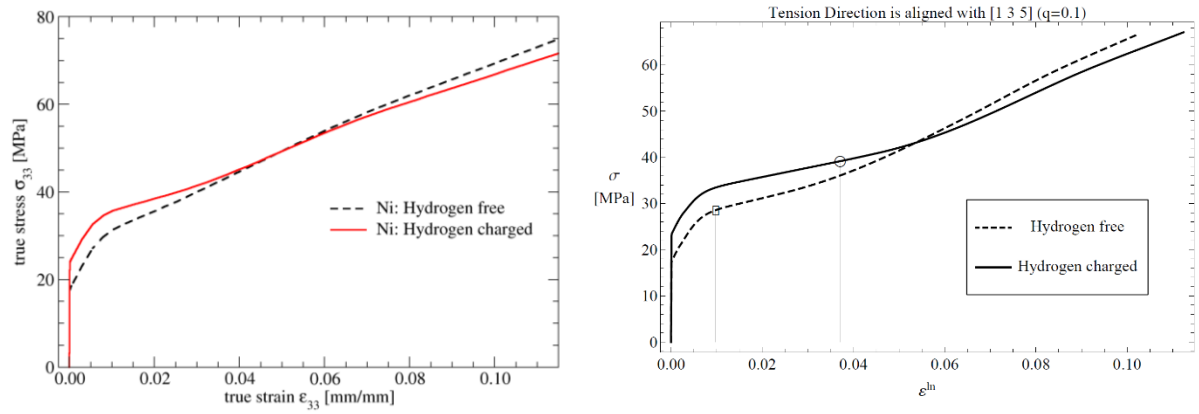

Figure 1: Macroscopic true stress-strain curves of hydrogen-free and hydrogen-charged Ni single crystal bar model. Left: this study. Right: previous study [17].

4 RESULTS (PRELIMINARY)

Several tensile test simulations are performed on the austenitic SS 316L polycrystalline model using different hydrogen concentrations to study the effect of dislocation-hydrogen interactions. Finite hydrogen concentrations result in an increased yield stress (due to activation of immobile dislocations) and reduced hardening with accompanied plastic strain localization (due to increase of dislocation mobility).

A fully periodic Voronoi-based polycrystalline model is generated with 100 grains of random crystallographic orientations (zero texture) and meshed by finite elements as shown in Fig. 2. The periodicity of the model is introduced to avoid the free-surface effects.

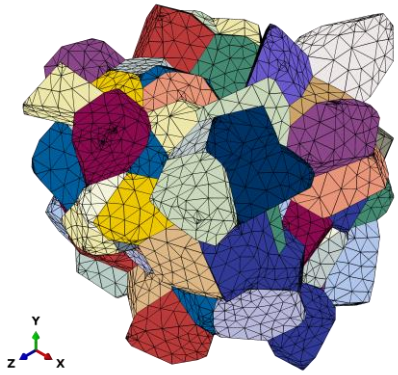

Figure 2: A fully periodic Voronoi tessellation with 100 grains (different colours) and the corresponding finite element mesh (42000 elements of C3D10 type) used in this study.

The material elasto-plastic parameters for austenitic SS 316L are taken from [6] while the hydrogen parameters of Ni from [10] are used as a first approximation (see Tab. 1 in Appendix).

In Fig. 3, the effect of varying T_c (controlling the yield stress) and H_c (controlling the softening) is demonstrated for a fixed total hydrogen concentration $c_0 = 0.015$. A clear influence of each of the parameters is shown.

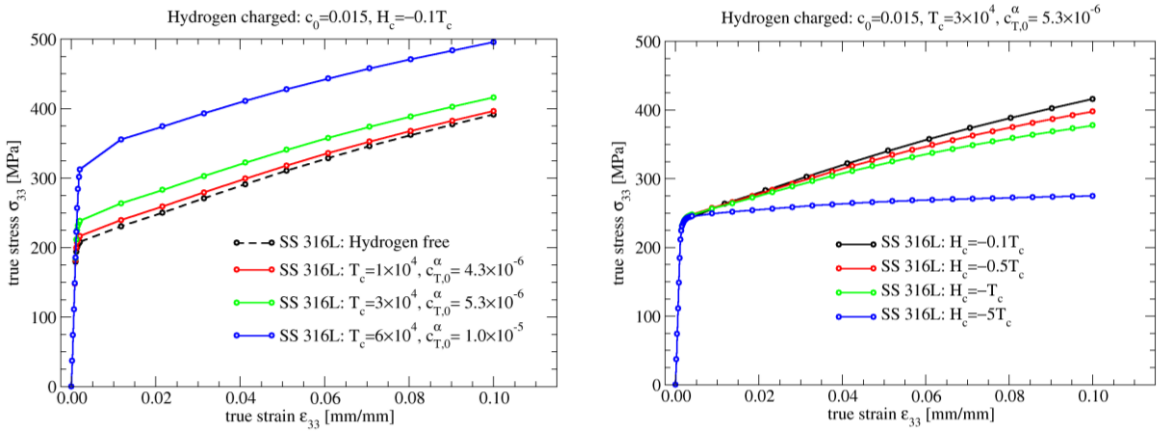

Figure 3: Macroscopic true stress-strain curves of hydrogen-free and hydrogen-charged austenitic SS 316L polycrystalline model. Left: effect of T_c (and the initial hydrogen trap concentration $c_{T,0}^{\alpha}$). Right: effect of H_c.

The effect of hydrogen on local strain distribution is shown in Figs. 4 and 5 for a polycrystalline SS 316L model under 0.10 tensile strain deformation. Indeed, a tendency of enhanced strain localization can be observed in the hydrogen-charged model, which qualitatively confirms the experimental observations [8]. However, further analysis is needed to quantify this effect in more detail and with better confidence.

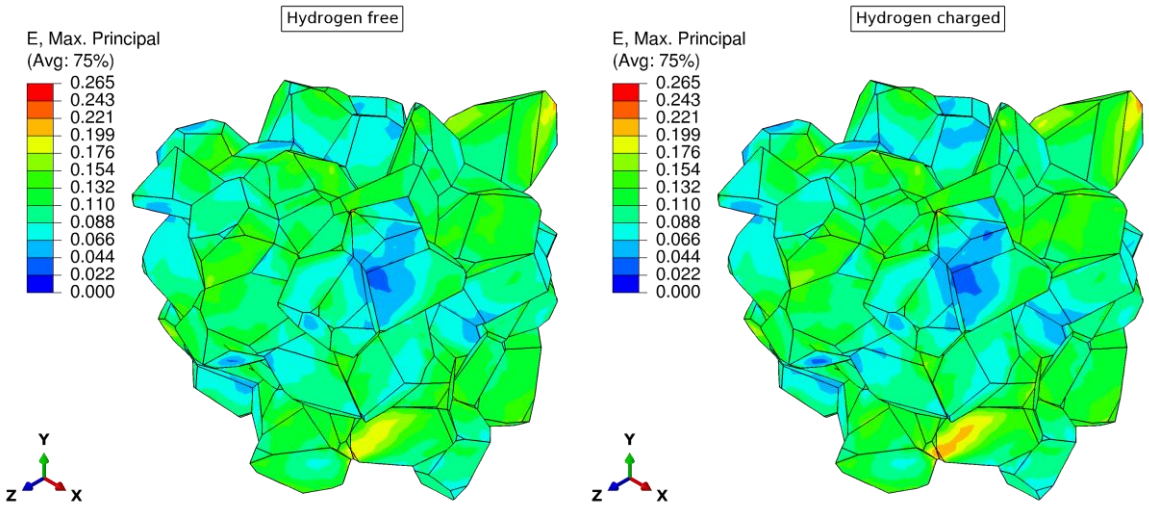

Figure 4: Maximum principal strain calculated for austenitic SS 316L polycrystalline model at macroscopic 0.10 tensile strain. Left: hydrogen free. Right: hydrogen charged (using the same parameters as for the green curve in Fig. 3 Right).

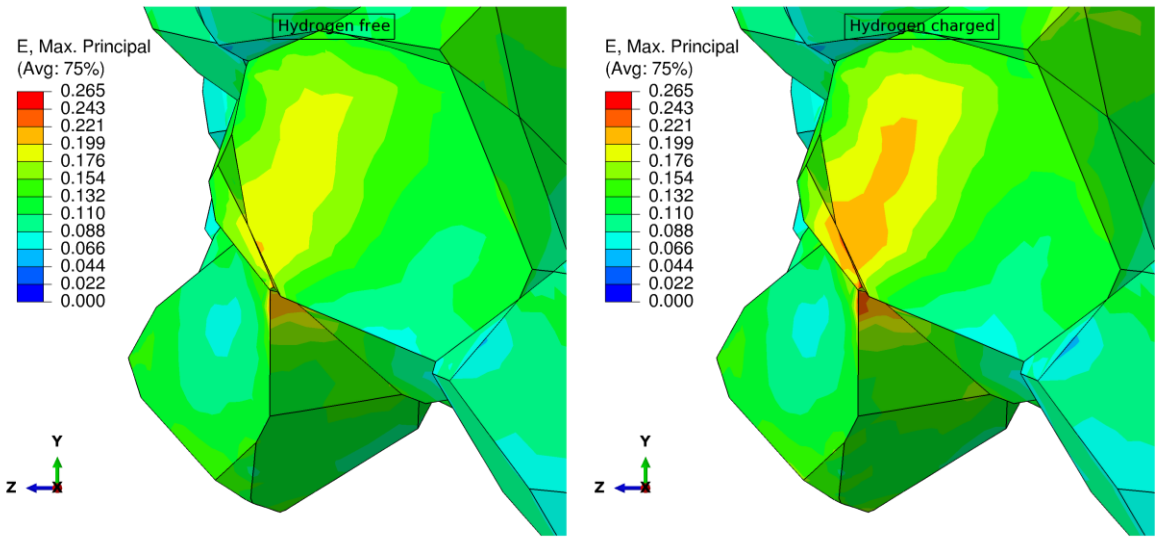

Figure 5: Enlarged part of Fig. 4. showing a tendency of strain localization in the hydrogen-charged polycrystalline model.

5 CONCLUSIONS

The effect of hydrogen concentration in polycrystalline austenitic stainless steel 316L has been studied in a series of tensile aggregate simulations. A rate-independent form of constitutive equations and corresponding tangent moduli have been derived in a finite strain formalism accounting for the dislocation-dislocation (Bassani-Wu hardening) and dislocation-hydrogen interactions. The derived equations have been successfully implemented in the User MATerial subroutine in Abaqus software. The preliminary results show an enhanced tendency of strain localization in hydrogen-charged models of polycrystalline austenitic stainless steel 316L.

ACKNOWLEDGMENTS

The authors gratefully acknowledge financial support provided by Slovenian Research Agency, Slovenia (grants P2-0026 and PR-12255).

APPENDIX

Table 1: Parameter values used in the analysis.

Parameter	Symbol	Value
Shear modulus	G	75.6 [GPa]
Burgers vector	b	0.249 [nm]
Molar volume of Ni	V_M	6.59 10^{-6} [m^3/mol]
Lattice atoms per unit volume	N_L	9.14 10^{28}[1/mm^3]
Proportionality constant	$\tilde{\alpha}$	0.3
Elasticity tensor coefficient	c_{11}	200 [GPa]
Elasticity tensor coefficient	c_{12}	136 [GPa]
Elasticity tensor coefficient	c_{44}	205 [GPa]
Initial hardening modulus	h_0	386 [MPa]
Hardening modulus during easy glide	h_s	70 [MPa]
Stage I stress	τ_I	97.9 [MPa]
Initial critical resolved shear stress	τ_0	82.8 [MPa]
Reference slip in Bassani-Wu hardening law	γ_0	0.018

Table 2: Symbol notation used in this study.

Symbol	Variable	Symbol	Variable
$\underset{\sim}{\sigma}$	Second order Cauchy stress	$\dot{\gamma}^{\alpha}$	Shear strain rate in slip system α
$\underset{\approx}{c}$	Fourth order elasticity tensor	$\underset{\sim}{s}_0^{\alpha}$	Slip direction vector in slip system α in reference configuration
$\underset{\sim}{\varepsilon}$	Second order infinitesimal strain	$\underset{\sim}{s}^{\alpha}$	Slip direction vector in slip system α in current configuration
$\underset{\sim}{\tau}$	Second order Kirchhoff stress tensor	$\underset{\sim}{m}_0^{\alpha}$	Normal direction vector of slip system α in reference configuration

$\underset{\approx}{L}$	Fourth order rate independent tangent modulus tensor	$\underset{\sim}{m}^{\alpha}$	Normal direction vector of slip system α in current configuration
$\underset{\approx}{L}^{e\tau}$, $\underset{\approx}{L}^{J}$	Elastic and plastic tangent modulus tensors	$\underset{\sim}{F}$	Second order total deformation gradient tensor
$\underline{v}$	Velocity vector	$\underset{\sim}{L}_i^p$	Second order plastic part of velocity gradient in intermediate configuration
$\underset{\sim}{D}$	Symmetric part of velocity gradient	X_i	Position in the reference configuration
x_i	Position in the current configuration		

REFERENCES

[1] M. Beauvy, G. Berthoud, M. Defranceschi, G. Ducros, D. Feron, Y. Guerin, C. Latge et al., Corrosion and alteration of materials from the nuclear industry, 2010, pp.50-56.

[2] J. M. Scherer, J. Besson, S. Forest, J. Hure, B. Tanguy, "Strain gradient crystal plasticity with evolving length scale: Application to voided irradiated materials", European Journal of Mechanics-A/Solids, 77, 2019, 103768.

[3] M. Aldo, L. Gélébart, S. Forest. "Intragranular localization induced by softening crystal plasticity: Analysis of slip and kink bands localization modes from high resolution FFT-simulations results", Acta Materialia, 175, 2019, pp. 262-275.

[4] C. Ling, B. Tanguy, J. Besson, S. Forest, F. Latourte, "Void growth and coalescence in triaxial stress fields in irradiated FCC single crystals", Journal of Nuclear Materials, 492, 2017, pp. 157-170.

[5] S. El Shawish, L. Cizelj, "Numerical investigation of grain misorientations at and close to the free surface of FCC polycrystalline metals", Computational Materials Science, 113, 2016, pp. 133-142.

[6] S. El Shawish, L. Cizelj, "Combining single-and poly-crystalline measurements for identification of crystal plasticity parameters: Application to austenitic stainless steel", Crystals, 7(6), 2017, pp.181.

[7] J. Hure, S. El Shawish, L. Cizelj, B. Tanguy, "Intergranular stress distributions in polycrystalline aggregates of irradiated stainless steel", Journal of Nuclear Materials, 476, 2016, pp. 231-242.

[8] D. Delafosse, "Hydrogen effects on the plasticity of face centred cubic (fcc) crystals. In Gaseous hydrogen embrittlement of materials in energy technologies", Woodhead Publishing, 285, 2012, pp. 247-285.

[9] Y. Yagodzinskyy, T. Saukkonen, S. Kilpeläinen, F. Tuomisto, H. Hänninen, “Effect of hydrogen on plastic strain localization in single crystals of austenitic stainless steel”, Scripta Materialia, 62(3), 2010, pp. 155-158.

[10] Y. Yagodzinskyy, O. Tarasenko, H. Hänninen, “Effect of hydrogen on plastic deformation of stable 18Cr-16Ni-10Mn austenitic stainless steel single crystals”, In International Conference on Hydrogen Effects on Material Behavior and Corrosion Deformation Interactions : MINERALS, METALS AND MATERIALS SOCIETY, 2003, pp. 201-210.

[11] D. P. Abraham, C. J. Altstetter, “The effect of hydrogen on the yield and flow stress of an austenitic stainless steel” Metallurgical and Materials transactions A, 26(11), 1995, pp. 2849-2858.

[12] M. E. Gurtin, E. Fried, L. Anand, The mechanics and thermodynamics of continua. Cambridge University Press, 2010.

[13] J. L. Bassani, T. Y. Wu, “Latent hardening in single crystals. II. Analytical characterization and predictions”, Proceedings of the Royal Society of London. Series A: Mathematical and Physical Sciences, 435(1893), 1991, pp. 21-41.

[14] G. J. Schebler, On the mechanics of the hydrogen interaction with single crystal plasticity, 2011.

[15] Oriani, R. A., “The diffusion and trapping of hydrogen in steel”, Acta metallurgica, 18(1), 1970, pp. 147-157.

[16] V. Singh, R. Kumar, Y. Charles, D. K. Mahajan, “Coupled diffusion-mechanics framework for simulating hydrogen assisted deformation and failure behavior of metals” International Journal of Plasticity, 157, 2022, 103392.

[17] N. Vasios, Crystal plasticity: A rate–independent constitutive model. The effect of Hydrogen concentration, 2015, pp. 117-120.